Electron-phonon superconductivity in APt_3P (A = Sr, Ca, La) compounds: From weak to strong coupling

Alaska Subedi, Luciano Ortenzi, and Lilia Boeri
Max Planck Institute for Solid State Research, Heisenbergstrasse 1, D-70569 Stuttgart, Germany
(Received 24 September 2012; revised manuscript received 13 March 2013; published 5 April 2013)

We study the newly discovered Pt phosphides APt_3P (A = Sr, Ca, La) [T. Takayama *et al.*, Phys. Rev. Lett. **108**, 237001 (2012)] using first-principles calculations and Migdal-Eliashberg theory. Given the remarkable agreement with the experiment, we exclude the charge-density wave scenario proposed by previous first-principles calculations, and give conclusive answers concerning the superconducting state in these materials. The pairing increases from La to Ca and Sr due to changes in the electron-phonon matrix elements and low-frequency phonons. Although we find that all three compounds are well described by conventional s-wave superconductivity and spin-orbit coupling of Pt plays a marginal role, we show that it could be possible to tune the structure from centrosymmetric to noncentrosymmetric opening new perspectives towards the understanding of unconventional superconductivity.

DOI: 10.1103/PhysRevB.87.144504 PACS number(s): 74.70.−b, 63.20.kd, 74.20.Pq

I. INTRODUCTION

In the last ten years, several important discoveries have sensibly advanced our understanding of superconductivity: a record T_c of 39 K in the BCS superconductor MgB_2,[1] exotic superconductivity with T_c of up to 56 K in the iron-based superconductors,[2] as well as superconductivity in boron-doped diamond,[3] aromatic compounds,[4] and so on. At the same time, ideas percolating from other fields of condensed matter have brought in new twists into this old and fascinating phenomenon. For example, the recent interest in spin-orbit coupling (SOC)[5] has revived the discussion on superconductivity in noncentrosymmetric crystals (NCSCs),[6,7] boosted by the discovery of the heavy fermion $CePt_3Si$ (T_c = 0.75 K) in 2004.[8] In crystals without inversion symmetry, a strong antisymmetric SOC that lifts the spin degeneracy can be conducive to exotic pairing symmetry. Because of the large SOC of Pt (Z = 78), this makes Pt-based compounds promising candidates for exotic superconductivity, as discussed for SrPtAs.[9,10]

Recently, Takayama *et al.* discovered a new family of ternary platinum phosphide superconductors with chemical formula APt_3P (A = Sr, Ca, and La) and T_c's of 8.4, 6.6, and 1.5 K, respectively.[11] Besides the relatively high T_c, these compounds exhibit a very interesting crystal structure, which is a centrosymmetric variant of the $CePt_3Si$ one. The authors have suggested that this discovery would have a very strong impact in the field of superconductivity if one could synthesize both centrosymmetric and noncentrosymmetric variants of superconductors consisting of the electronically equivalent elements. This would in fact allow us to study the effect of inversion symmetry on superconductivity in a controlled way. The nature of the superconducting pairing in the APt_3P compounds has been debated through experiments[11] and *ab initio* calculations.[12–14] In the original discovery paper, it was proposed that, at least in $SrPt_3P$, the superconductivity is of strong-coupling s-wave type with clear signatures of low-lying phonons and large BCS ratios suggestive of multiband behavior. Reference 13 has instead proposed that T_c is enhanced by the proximity to a dynamical charge-density wave (CDW) instability, and that a strong SOC could eventually lead to *exotic* superconductivity in $LaPt_3P$. Reference 14 found no indication of CDW instability, and supported a conventional electron-phonon (EP) scenario.

In this paper, we employ first-principles calculations and Migdal-Eliashberg theory to study superconductivity in the APt_3P phosphides. We find that SOC plays a marginal role in all three compounds and show that the available experimental data are quantitatively reproduced by conventional EP theory, based on well-converged electronic and phonon spectra. This rules out exotic pairing and CDW instabilities.[13] In fact, the APt_3P series is a textbook example for EP superconductivity: $LaPt_3P$, where T_c is only 1.5 K, is a typical low-T_c superconductor in which all phonon branches are moderately coupled to the electrons at E_F. Lowering the electronic filling from trivalent La to divalent Sr and Ca brings about an intense EP coupling that is concentrated in low-lying phonon branches with substantial Pt in-plane breathing character. In $SrPt_3P$, these branches are flat and have low frequencies, and this entirely explains the large value of its BCS ratios,[11,15] with no need for multiband effects.

II. METHODS

Our calculations employ density functional perturbation theory,[16] within the generalized gradient approximation (GGA) as implemented in the Quantum-ESPRESSO package.[17] We use ultrasoft pseudopotentials[18] and basis set cutoffs of 40 and 400 Ry for wave function and charge density, respectively. We use an $8 \times 8 \times 8$ grid for zone integration in the self-consistent calculations, while a denser $16 \times 16 \times 16$ grid is used in the electron-phonon coupling calculations. The dynamical matrices are calculated on an $8 \times 8 \times 8$ grid, and phonon dispersions and density of states (DOS) are then obtained by Fourier interpolation. The results of the structural relaxation were tested with the all-electron code WIEN2K, which employs the full potential linear augmented plane-wave method.[19,20]

III. STRUCTURE

Figure 1(a) shows the crystal structure of the APt_3P phosphides (space group $P4/nmm$). In these tetragonal antiperovskites, the ionic radii of Pt and P ions are similar, and

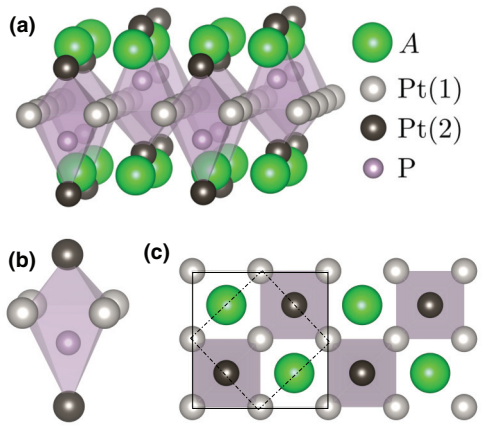

FIG. 1. (Color online) (a) Crystal structure of $A\mathrm{Pt_3P}$, space group $P4/nmm$. The $\sqrt{2}\times\sqrt{2}$ in-plane arrangement of the distorted $X\mathrm{Pt_6}$ octahedra (b) distinguishes the $A\mathrm{Pt_3P}$ compounds from the noncentrosymmetric $\mathrm{CePt_3Si}$ superconductor (space group $P4mm$); the corresponding unit cells are shown as full and dashed lines in panel (c).

the P ions are off center from the octahedral basal plane formed by the Pt(1) ions as the P ion is too big to fit into the center of the Pt(1) square. The apical Pt(2) ion that is further from the P ion also moves closer to the basal plane to ensure closer packing of the constituent ions. The distortion of the $X\mathrm{Pt_6}$ octahedra occurs in both the phosphides (X = P) and in the noncentrosymmetric rare-earth silicides $\mathrm{CePt_3Si}$ and $\mathrm{LaPt_3Si}$ (X = Si), with space group $P4mm$. What distinguishes the two structures is the in-plane arrangement of the octahedra. In the silicides, the distortions have a *polar* arrangement, i.e., they all point in the same direction, and the resulting structure has no inversion symmetry. The corresponding unit cell that contains one formula unit (f.u.) is shown with dashed lines in Fig. 1(c). With full lines we show the $\sqrt{2}\times\sqrt{2}$ cell of the phosphides, where the distortions alternate in a checkerboard fashion and restore the inversion symmetry (*antipolar* structure). Therefore, the unit cell comprises two f.u., and A, Pt(1), Pt(2), and P occupy $2a$, $4e$, $2c$, and $2c$ Wyckoff positions, respectively. We relaxed the structures fully within GGA such that the force on each atom is less than 10^{-5} Ry/bohr. The relaxed parameters are given in Table I.

The crystal structure of $A\mathrm{Pt_3P}$, with space group $P4/nmm$, and that of $\mathrm{REPt_3Si}$ (RE = La, Ce), with space group $P4/mm$, can be seen as variants of the same antiperovskite structure, which differ only for the in-plane polar arrangement of the distorted $X\mathrm{Pt_6}$ octahedra. For A = La both the noncentrosymmetric ($P4/nmm$) silicide and the centrosymmetric ($P4/mm$) phosphide compound exist, and are superconducting with low

TABLE I. Fully relaxed structural parameters (GGA) for the $A\mathrm{Pt_3P}$ compounds in the experimental $P4/nmm$ structure.

	a (Å)	c (Å)	z_{Pt2}	z_{P}
$\mathrm{SrPt_3P}$	5.898	5.470	0.1362	0.7227
$\mathrm{CaPt_3P}$	5.758	5.494	0.1357	0.7303
$\mathrm{LaPt_3P}$	5.838	5.553	0.1418	0.7719

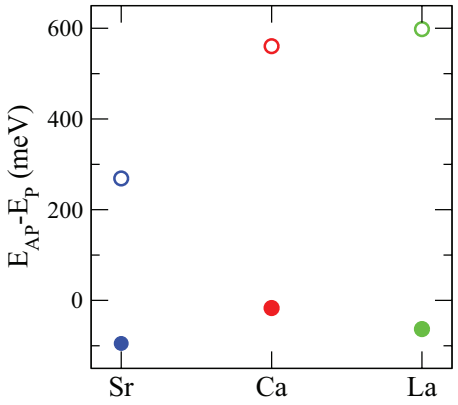

FIG. 2. (Color online) Total-energy difference between the antipolar and polar structure for phosphides (full symbols) and selenides (empty symbols), in the fully relaxed GGA structure at zero pressure.

T_c's $\lesssim$ 2 K, while for A = Sr, Ca to our knowledge only the phosphides have been synthesized.

We have studied the relative stability of the two structures for $A\mathrm{Pt_3}$ silicides and phosphides, using total-energy calculations. The structures were fully relaxed in GGA at zero pressure. For the existing compounds, the relaxed parameters are within ~2% of the experimental values.

In Fig. 2, we plot the difference in total energies between the antipolar and polar structures ($E_{AP} - E_P$). The difference is negative for phosphides (full symbols), and positive for silicides (empty symbols), with approximately an order of magnitude difference between the two cases. The small energy differences found in the phosphides (a few tens meV), and in particular for $\mathrm{CaPt_3P}$, indicates that it might be indeed possible to synthesize these compounds also in the *polar* variant, realizing the proposal of Takayama *et al.* to study the lack of inversion symmetry in electronically equivalent compounds.[11]

IV. ELECTRONIC STRUCTURE

In the following, we stick to the $A\mathrm{Pt_3P}$ compounds in the $P4/nmm$ structure, employing fully relaxed lattice constants and internal parameters. Our electronic structures are in very good agreement with previous calculations.[12,13] A zoom-in of the bands for energies ±1 eV around the Fermi level (E_F), with (red, dashed) and without (black, solid) SOC, is shown in Fig. 3. Only in $\mathrm{LaPt_3P}$ does the SOC lead to a visible lifting of some band degeneracies. But even in this case, the bands remain spin degenerate, in contrast to what is claimed by Ref. 13. Since the SOC plays only a marginal role on the electronic states near E_F, we neglect it in the following.

Figure 4 shows the "fat" bands without the SOC of the three $A\mathrm{Pt_3P}$ compounds, highlighting the orbital characters which give the highest contribution to the electronic states at the Fermi surface. The axes are oriented along the shortest in-plane Pt-Pt distance. The Fermi surface of the A^{2+} compounds comprises a large, low dispersive sheet, formed by the band with prominent Pt(1) $d_{x^2-y^2}$ character which crosses E_F along the $\Gamma - X - M$ line; two other bands, with more Pt(2), P and interstitial character, form two more dispersive pockets, i.e., a large, flat, structure centered around the Γ point, and a small

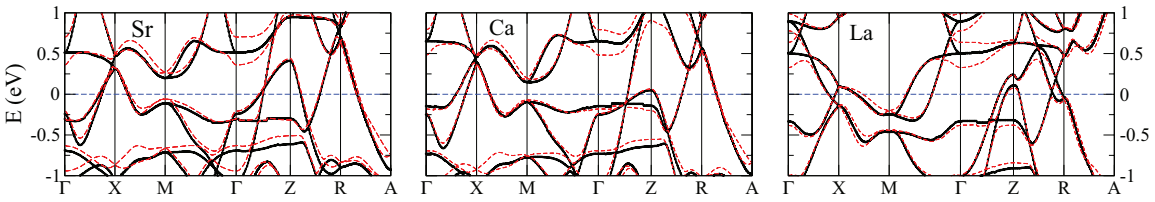

FIG. 3. (Color online) Electronic structure of APt$_3$P with (red, dashed line) and without (black, solid line) spin-orbit coupling (SOC); the zero of the energy is the Fermi level.

cigar-shaped hole pocket around the Z point. These bands cross E_F along the $Z - R - A$ line. This unequal distribution of orbital characters on the Fermi surface suggests that the superconducting gap may be anisotropic. LaPt$_3$P, with one more electron per f.u. has its Fermi level shifted up by ∼0.5 eV, and the band with low dispersion along $M - \Gamma$ is completely full. The Fermi surface is composed of highly dispersive sheets, with strongly mixed orbital contributions of Pt(2), P, and Pt(1) characters.

V. PHONON DISPERSIONS AND ELECTRON-PHONON COUPLING

The three compounds have very similar phonon dispersions, shown in the left panels of Fig. 5. The 30 phonon branches extend up to ∼450 cm^{-1}, with two upper branches of mostly out-of-plane P character, four intermediate branches at ∼300 cm^{-1} that show mostly in-plane vibration of P, and a lower manifold of the 24 strongly intertwined branches, with mixed A, Pt(1), and Pt(2) character.

There is a substantial difference in the three Eliashberg functions $\alpha^2F(\omega)$, plotted in the rightmost panels of Fig. 5 and defined as

$$\alpha^2F(\omega) = \frac{1}{N(0)} \sum_{\mathbf{k},\mathbf{q},\nu,n,m} \delta\left(\epsilon^n_{\mathbf{k}}\right)\delta\left(\epsilon^m_{\mathbf{k}+\mathbf{q}}\right)\left|g^{\nu,n,m}_{\mathbf{k},\mathbf{k}+\mathbf{q}}\right|^2\delta\left(\omega-\omega^\nu_{\mathbf{q}}\right), \tag{1}$$

where $\omega^\nu_{\mathbf{q}}$ are phonon frequencies, $\epsilon^n_{\mathbf{k}}$ are electronic energies, and $g^{\nu,n,m}_{\mathbf{k},\mathbf{k}+\mathbf{q}}$ are EP matrix elements. The $\alpha^2F(\omega)$ yield information not only on the intensity of the total EP coupling (EPC) λ, but also on the nature of the bonding and character of the superconducting state. In general, an $\alpha^2F(\omega)$ roughly proportional to the PDOS is characteristic of metals with a weak to moderate total coupling and low $T_c's \lesssim 5$ K. The best EP superconductors, such as MgB_2 and A15's, are instead characterized by $\alpha^2F(\omega)$ which display sharp peaks only at specific parts of the phonon spectrum, reflecting a strong coupling between specific electron and phonon states. This requires (partly) covalent bonding. It is not uncommon that within the same family of materials the electron count changes

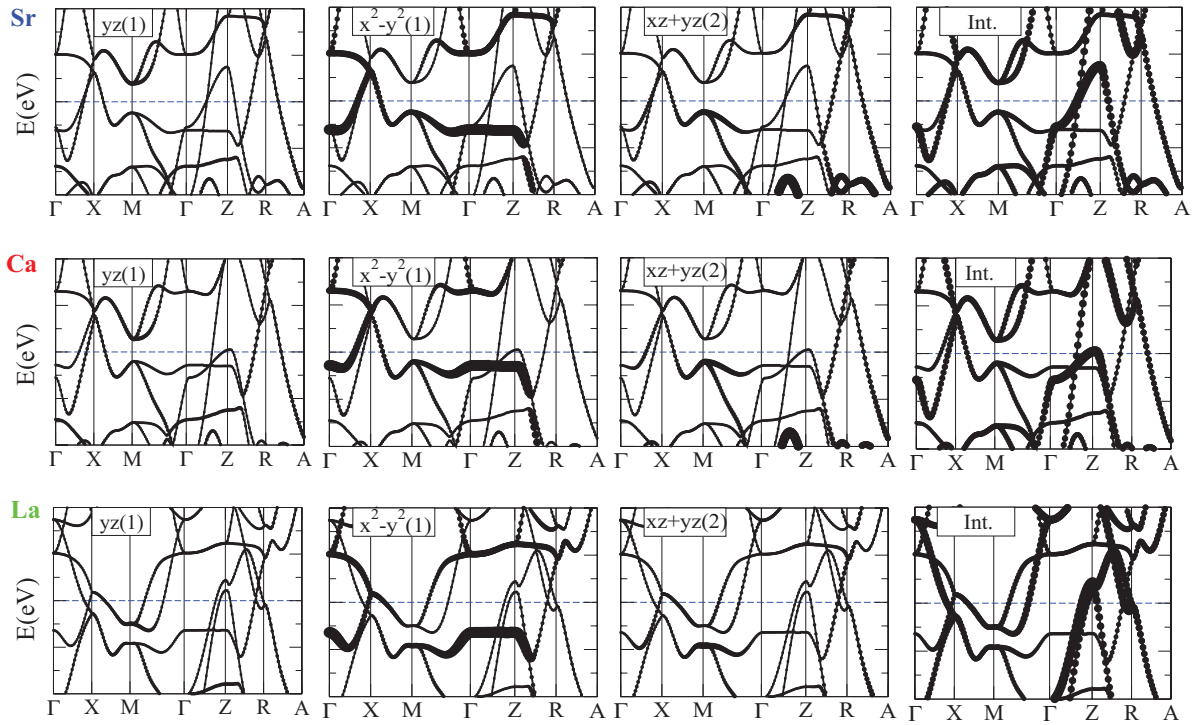

FIG. 4. (Color online) "Fat bands" of APt$_3$P, decorated with partial orbital characters. $xy(1)$ and $yz(1)$ are in-plane Pt [Pt(1)] partial characters; $yz(2)$ refers to Pt apical atoms [Pt(2)]; Int is interstitial.

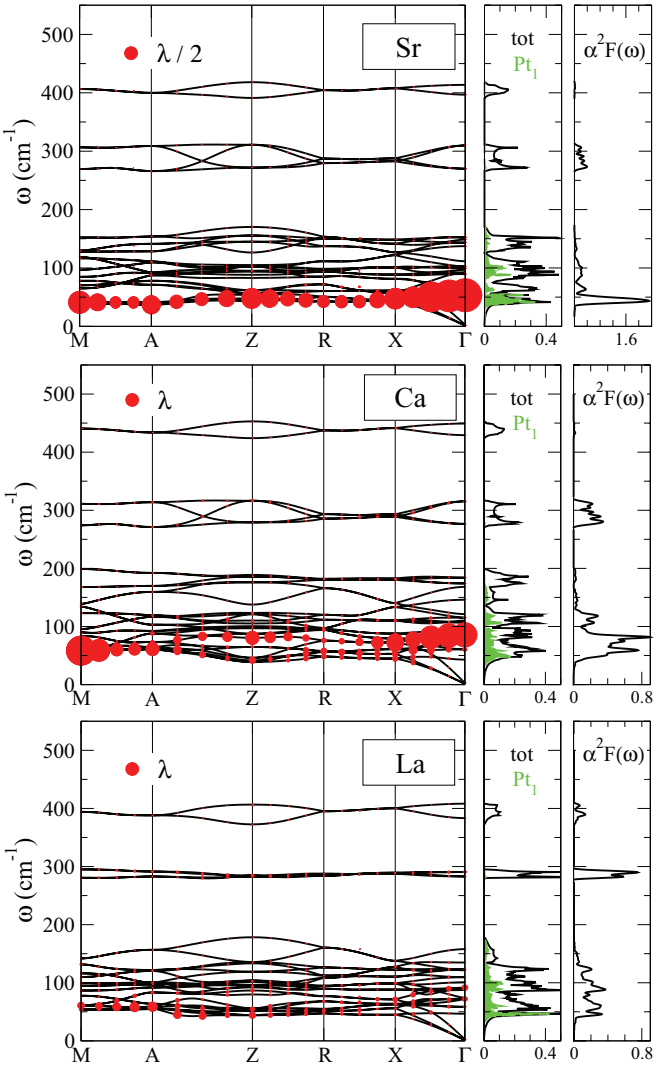

FIG. 5. (Color online) Phonon dispersions, density of states, and Eliashberg function $\alpha^2F(\omega)$ of APt_3P. The phonon dispersions are decorated with symbols, proportional to the partial EP coupling $\lambda_{\mathbf{q}\nu}$; for readability, the λ's for Sr have been rescaled by a factor of 2. The logarithmically averaged phonon frequencies $\omega_{\ln}$, the EP coupling constants λ, and the corresponding critical temperatures T_c's are given in Table III.

the EP coupling regime from weak to strong, depending on the nature of the electronic states at E_F selected by the two δ functions in Eq. (1).

Figure 5 shows that while the coupling is uniform in $LaPt_3P$, in the two A^{2+} compounds it is strongly enhanced at low frequencies. Furthermore, it is almost entirely concentrated in the low-lying phonon branches with substantial Pt(1) in-plane breathing character, which at the Γ point has B_{2u} symmetry—$\omega^{\rm br}_{\mathbf{q}}$ in the following.[13,14] These modes are very low in energy and almost dispersionless in $SrPt_3P$ ($\omega \sim 50$ cm^{-1}) and slightly harder in Ca, where they have a sizable dispersion that extends up to $\sim$100 cm^{-1}. One can trace their evolution in the two compounds by following the largest $\lambda^{\nu}_{\mathbf{q}}$ symbols that decorate the phonon dispersions, or looking at the partial Pt(1) phonon DOS plotted in the middle panel of Fig. 5. In-plane Pt breathing modes couple more strongly to the Pt(1) in-plane

TABLE II. Some calculated results for APt_3P: Electronic density of states at the Fermi level $N(0)$ in states/eV/spin/unit cell; $\omega_{\ln}$ in K; frequency $\omega^{\rm br}$ in cm^{-1}, e-ph coupling $\lambda^{\rm br}$, and e-ph coupling strength $I^{\rm br}$ in cm^{-2} for the in-plane Pt(1) breathing mode at Γ.

	$N(0)$	λ	$\omega_{\ln}$	$\omega^{\rm br}$	$\lambda^{\rm br}$	$I^{\rm br}$
$SrPt_3P$	2.36	1.33	77	53.0	1.90	5337
$CaPt_3P$	2.37	0.85	110	85.5	0.63	4605
$LaPt_3P$	1.94	0.57	118	91.5	0.14	1172

electronic states, and less to other partial characters. This causes some anisotropy in the $\mathbf{k}$ space distribution of the EPC and, as a consequence, in the $\mathbf{q}$ dependence of the $\lambda^{\nu}_{\mathbf{q}}$ in the $A^{2+}Pt_3P$, and explains the much lower coupling in $LaPt_3P$.

The total EPC constant $\lambda = \sum_{\mathbf{q},\nu} \lambda^{\nu}_{\mathbf{q}} = 2\int_0^{\infty} \frac{\alpha^2F(\omega)}{\omega} d\omega$ is quite low in $LaPt_3P$ ($\lambda = 0.57$) but sizable both in $CaPt_3P$ ($\lambda = 0.85$) and $SrPt_3P$ ($\lambda = 1.33$). Due to the $1/\omega$ factor, the EPC is strongly enhanced in $SrPt_3P$ with respect to $CaPt_3P$ because a considerable part of the breathing branches is shifted to low frequencies. A similar softening of the breathing branch is discussed by Chen *et al.*,[13] who find a dynamical instability of the breathing branch, which we cannot reproduce.[21] For some $\mathbf{q}$ points where the differences in $\omega^{\rm br}_{\mathbf{q}}$ are large, the partial EPC constants $\lambda^{\rm br}_{\mathbf{q}} = \text{const} \times I^{\rm br}_{\mathbf{q}}/(\omega^{\rm br}_{\mathbf{q}})^2$ differ by as much as a factor of 3 despite a very small difference ($\sim$10%) in the matrix elements ($I^{\rm br}$), as shown in Table II for the Γ point.

The small difference in the EP matrix elements implies that the lowering of the frequencies in Sr with respect to Ca is not due to increased EP coupling. Rather, this is almost entirely a structural effect, since we find that $\omega^{\rm br}_{\mathbf{q}}$ is increased (reduced) by reducing (increasing) the in-plane lattice constant, which in $CaPt_3P$ is $\sim$0.14 Å smaller than in $SrPt_3P$. To confirm the strong sensitivity of the Pt(1) breathing branch to the in-plane lattice constant, we have calculated the Γ-point phonon frequencies of $SrPt_3P$ as a function of pressure using the theoretical structures that are optimized within the GGA. The frequency of the B_{2u} mode as a function of pressure is plotted in Fig. 6 together with the corresponding value of the in-plane lattice constant a. For pressures of $\pm$4 GPa, we estimate a linear dependence $\omega^{\rm br}(P) = +5$ cm^{-1}/GPa. This translates into an almost linear dependence in terms of the in-plane lattice constant: $\omega^{\rm br}(a) \sim -20$ cm^{-1}/Å. From the calculated pressure derivative of the zone-center frequency of $SrPt_3P$, we estimate that this would

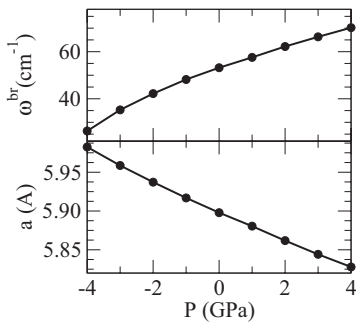

FIG. 6. $SrPt_3P$: Calculated frequency of the B_{2u} mode of $SrPt_3P$ (top) and in-plane lattice constant (bottom) as a function of pressure.

correspond to a 30-cm^{-1} hardening of the phonon frequency, in remarkable agreement with the values calculated for $CaPt_3P$.

The sensitivity of $\omega_{\mathbf{q}}^{\mathrm{br}}$ to the value of the in-plane lattice constant explains why the regime for superconductivity is weak coupling in Ca and strong coupling in Sr, despite the very close critical temperatures. In fact, the shift of spectral weight in $\alpha^2F(\omega)$ to lower energies causes a strong enhancement in λ, but it also induces a decrease in $\omega_{\ln} = \exp[\frac{2}{\lambda}\int_0^\infty d\omega/\omega\alpha^2F(\omega)\ln\omega]$—see Table II. These two factors compensate in the Allen-Dynes expression for T_c:

$$T_c = \frac{\omega_{\ln}}{1.20}\exp\left(-\frac{1.04(1+\lambda)}{\lambda-\mu^*-0.62\lambda\mu^*}\right),$$

but not in the BCS ratios ($2\Delta/T_c$, $\Delta C/T_c$, etc.), which to a very good approximation depend only on the quantity $T_c/\omega_{\ln}$.

VI. MIGDAL-ELIASHBERG THEORY

In Ref. 15 Marsiglio and Carbotte have shown that the BCS ratios of all known superconductors fall on a universal curve when plotted as a function of $T_c/\omega_{\ln}$. We have obtained the values of the superconducting and thermodynamical quantities from the full solution of the single-band Migdal-Eliashberg equations to locate the APt$_3$P compounds on the Marsiglio-Carbotte plots. As shown in Fig. 7 and from the data summarized in Table III, $LaPt_3P$ and $CaPt_3P$, with $T_c/\omega_{\ln} = 0.013$ and 0.058, respectively, lie together with elemental metals, while $SrPt_3P$ ($T_c/\omega_{\ln} = 0.110$) is placed at the lower end of a broad class of the low-phonon, strong-coupling superconductors, together with the A15 and Chevrel compounds.

In order to calculate the critical temperatures, gap values and specific-heat data presented in Fig. 7 and Table III we solved the Migdal-Eliashberg equations[22] in the single-band

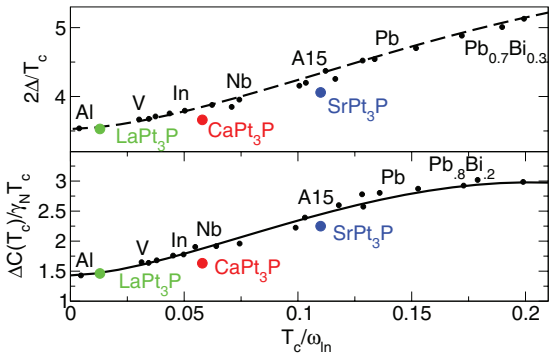

FIG. 7. (Color online) Location of the APt$_3$P compounds on the Marsiglio-Carbotte plots for strong-coupling superconductors. Δ is the superconducting gap at zero temperature, T_c is the critical temperature, $\Delta C(T_c)$ is the jump in the electronic specific heat at T_c, γ is the linear coefficient of the normal-state specific heat, obtained from DFT and single-band Migdal-Eliashberg theory, and $\omega_{\ln}$ is the logarithmic averaged phonon frequency (see text). Lines are obtained from approximate solution of the Migdal-Eliashberg equations. Figures are adapted from Ref. 15. In increasing order the black points correspond to the following systems: Al, V, Ta, Sn, Tl, In, Nb (Butler), Nb (Arnold), Nb (Robinson), $Nb_{0.75}Zr_{0.25}$, V_3Ga,Nb_3Al, Nb_3Ge, Pb, $Pb_{0.8}Tl_{0.2}$, $Pb_{0.9}Bi_{0.1}$, $Pb_{0.8}Bi_{0.2}$, $Pb_{0.7}Bi_{0.3}$, and $Pb_{0.65}Bi_{0.35}$. Data taken from Ref. 15, and references cited therein.

TABLE III. Superconducting properties of APt$_3$P, from first-principles calculations and Migdal-Eliashberg theory; γ_N is the electronic normal-state specific heat, in mJ mol^{-1} K^{-2}, $\Delta(0)$ is the value of the superconducting gap, ΔC is the specific heat jump at T_c. Experimental data from Ref. 11 are in parentheses. The Coulomb pseudopotential μ^* was fixed to reproduce the experimental T_c.

	γ_N	T_c	$2\Delta(0)/T_c$	$\Delta C/T_c$	$T_c/\omega_{\ln}$	μ^*
Sr	12.9 (12.7)	8.5 (8.4)	4.06	29.0 (28)	0.110	0.11
Ca	10.3 (17.4)	6.34 (6.6)	3.66	16.8 (11)	0.058	0.09
La	7.18 (6.7)	1.56 (1.5)	3.53	10.5 (2)	0.013	0.11

case:

$$\phi(\omega_n) = \pi T\sum_{m=-M}^{m=M}[\lambda(\omega_n-\omega_m)-\mu^*] \times \frac{\phi(\omega_m)}{\sqrt{\omega_m^2Z^2(\omega_m)+\phi^2(\omega_m)}},$$

$$Z(\omega_n)\omega_n = \omega_n + \pi T\sum_{m=-M}^{m=M}\lambda(\omega_n-\omega_m) \times \frac{Z(\omega_m)\omega_m}{\sqrt{\omega_m^2Z^2(\omega_m)+\phi^2(\omega_m)}}$$

$$\lambda(\omega_n-\omega_m) = 2\int_0^\infty \frac{\Omega\alpha^2F(\Omega)d\Omega}{(\omega_n-\omega_m)^2+\Omega^2},$$

where $\phi(\omega_n) = \Delta(\omega_n)Z(\omega_n)$, $\Delta(\omega_n)$ is the superconducting gap, $Z(\omega_n)$ is the mass enhancement factor, and M is the number of Matsubara frequencies ω_n used in the calculations. We used the Eliashberg functions in Fig. 5 and the densities of states in Table II. The value of μ^* was chosen to reproduce the experimental T_c—we obtained $\mu^* = 0.1 \pm 10\%$ for all three compounds—and kept fixed in the calculations of the specific-heat jump and superconducting gap. The specific-heat jump was obtained by numerically calculating the difference $\Delta F(T)$ between the normal state (N) free energy and the superconducting one (S):[23]

$$\Delta F(T) = -\pi T\sum_{m=-M}^{m=M}\left\{|\omega_n|[Z_N(\omega_n)-1] - \frac{2\omega_n^2\left[Z_S^2(\omega_n)-1\right]+2\phi^2(\omega_n)}{|\omega_n|+\sqrt{\omega_n^2Z_S^2(\omega_n)+\phi^2(\omega_n)}} + \frac{\omega_n^2Z_S(\omega_n)[Z_S(\omega_n-1)]+\phi^2(\omega_n)}{\sqrt{\omega_n^2Z_S^2(\omega_n)+\phi^2(\omega_n)}}\right\}$$

and fitting the obtained curve with a 12th-order polynomial. The specific heat was then obtained from the second derivative of the polynomial expansion.

Figure 8 shows a comparison of the specific-heat data with experiments from Ref. 11. In the inset, we compare calculations (solid lines) and experiments (symbols) for the total normal-state specific heat of $SrPt_3P$. The lattice specific heat is fitted with $c(T) = bT^3 + dT^5$, $b = 1.29(1.26)$ mJ/mol K^4,

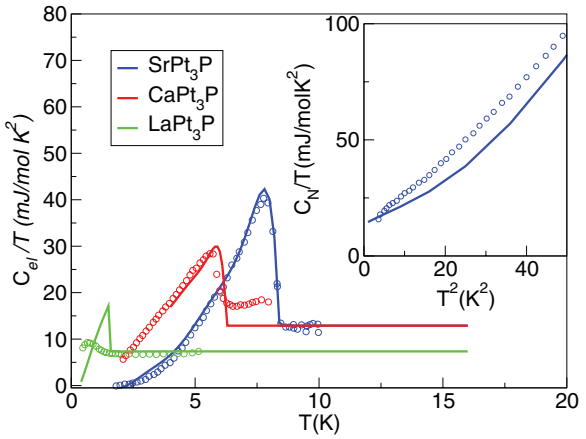

FIG. 8. (Color online) Comparison between experimental data from Ref. 11 (colored dots) and Migdal Eliashberg theory (colored lines) for the heat capacities of APt_3P (A = Sr, Ca, and La). Inset: Comparison between experimental data from Ref. 11 (blue dots) and first-principles calculations (blue line) for the normal-state specific heat of $SrPt_3P$.

$d = 8.9(13.0)$ mJ/mol K^6 for theoretical (experimental) data, respectively. This remarkable agreement suggests that our calculated phonon spectra, with a sharp peak at $\omega \sim 50$ cm^{-1}, are very close to the actual ones. This allow us to rule out the dynamical instabilities calculated in Ref. 13.

In the main panel of Fig. 8, the superconducting state data for $SrPt_3P$ are shown as a blue curve. The single-band Migdal-Eliashberg calculations, which yield $\frac{2\Delta}{T_c} \sim 4.06$, reproduce almost exactly the experimental curve. Âs for the low-T_c compounds, we again obtain critical temperatures in very good agreement with experiments, with $\mu^* = 0.1$, which is a strong indication in favor of conventional superconductivity. $CaPt_3P$ (red curves in Fig. 8) displays a mass enhancement in the normal state that is 2.5 times larger than the calculated one, which we attribute to the presence of additional superconducting phases in the sample. All other quantities are in line with our calculations. In fact, using the calculated value of $\gamma_N = 10.3$ mJ mol^{-1} K^{-2}, we obtain also a reasonable fit to the specific heat jump, as shown in Fig. 8. For $LaPt_3P$ (green curves in Fig. 8) we obtain a fairly good agreement for the normal-state quantities, while the superconducting state data are probably too noisy for a meaningful comparison.

Figure 7 clearly shows that the values we obtain for all three APt_3P compounds are fully in line with other EP superconductors. The very high BCS ratio $2\Delta/T_c = 5.0$ reported from Takayama *et al.*[11] for $SrPt_3P$ lies instead out of the general trend. In Fig. 7, $2\Delta/T_c = 5.0$ corresponds to $T_c/\omega_{\ln} \sim 0.18$, which, given the calculated $\omega_{\ln}$, leads to a $T_c \sim 14$ and $\lambda \sim 3$, clearly inconsistent with the experiment. In Ref. 11 the value $2\Delta/T_c = 5.0$ is one of the strongest arguments for multiband superconductivity. We believe that this is an artifact of the simplified α model used by the authors to fit the experimental specific heat. In fact, as we have shown above, a single gap Migdal Eliashberg model perfectly fits the electronic specific heat for $SrPt_3P$, with a lower $2\Delta/T_c = 4.06$. Therefore, also the possible anisotropy in the gap suggested by the uneven distribution of orbital characters on the Fermi surface is either negligible, or washed out by impurities in real samples. At the same time, the good agreement of the calculated lattice specific heat allows us to rule out the dynamical instability of the low-lying phonon branches in $SrPt_3P$ and the CDW scenario based thereon.[13] The same single-band analysis, applied to the lower T_c compounds, yields critical temperatures in very good agreement with experiments, which is a strong indication in favor of conventional superconductivity.

VII. CONCLUSIONS

In conclusion, the first-principles calculations and Migdal-Eliashberg analysis presented in this work allow us to make some conclusive statements about the nature of superconductivity in the recently discovered APt_3Pt compounds (A = Sr, Ca, La).[11] Superconductivity in APt_3Pt (A = Sr, Ca, La) compounds is of conventional EP nature and the SOC plays a negligible role, thus ruling out the proposals of exotic superconductivity of Refs. 12 and 13. The electronic filling brings about an EP coupling which is moderate in La, and much stronger in Ca and Sr, where Pt(1) breathing phonons couple to in-plane electronic states. The frequency and dispersion of the breathing phonons can be *tuned* acting on the in-plane lattice constant, leading to weak- and strong-coupling values of the BCS ratios in Ca and Sr, despite the very close critical temperatures.

Furthermore, our total-energy calculations suggest that the APt_3P compounds could also be synthesized in the related, noncentrosymmetric $CePt_3Si$ structure, through appropriate synthesis conditions or partial replacement of P with Si. This would realize the original proposal of Takayama *et al.*,[11] and open the way to the exciting possibility of studying the effect of the lack of inversion symmetry on superconductivity in a *controlled* way.

ACKNOWLEDGMENTS

We would like to acknowledge A. P. Schnyder, O. V. Dolgov, and R. K. Kremer for useful discussions.

[1] J. Nagamatsu, N. Nakagawa, T. Muranaka, Y. Zenitani, and J. Akimitsu, Nature (London) **410**, 63 (2001).
[2] Y. Kamihara, T. Watanabe, M. Hirano, and H. Hosono, J. Am. Chem. Soc. **130**, 3296 (2008).
[3] E. A. Ekimov, V. A. Sidorov, E. D. Bauer, N. N. Mel'nik, N. J. Curro, J. D. Thompson, and S. M. Stishov, Nature (London) **428**, 542 (2004).
[4] R. Mitsuhashi, Y. Suzuki, Y. Yamanari, H. Mitamura, T. Kambe, N. Ikeda, H. Okamoto, A. Fujiwara, M. Yamaji, N. Kawasaki, Y. Maniwa, and Y. Kubozono, Nature (London) **464**, 76 (2010).
[5] B. J. Kim, H. Jin, S. J. Moon, J.-Y. Kim, B.-G. Park, C. S. Leem, J. Yu, T. W. Noh, C. Kim, S.-J. Oh, J.-H. Park, V. Durairaj, G. Cao, and E. Rotenberg, Phys. Rev. Lett. **101**, 076402 (2008); M. Z. Hasan and C. L. Kane, Rev. Mod. Phys. **82**, 3045 (2010).

[6]M. Sigrist and K. Ueda, Rev. Mod. Phys. **63**, 239 (1991).
[7]M. H. Fischer, F. Loder, and M. Sigrist, Phys. Rev. B **84**, 184533 (2011).
[8]E. Bauer, G. Hilscher, H. Michor, Ch. Paul, E. W. Scheidt, A. Gribanov, Yu. Seropegin, H. Noël, M. Sigrist, and P. Rogl, Phys. Rev. Lett. **92**, 027003 (2004).
[9]Y. Nishikubo, K. Kudo, and M. Nohara, J. Phys. Soc. Jpn. **80**, 055002 (2011).
[10]S. J. Youn, M. H. Fischer, S. H. Rhim, M. Sigrist, and D. F. Agterberg, Phys. Rev. B **85**, 220505 (2012); J. Goryo, M. H. Fischer, and M. Sigrist, Phys. Rev. B **86**, 100507(R) (2012).
[11]T. Takayama, K. Kuwano, D. Hirai, Y. Katsura, A. Yamamoto, and H. Takagi, Phys. Rev. Lett. **108**, 237001 (2012).
[12]I. A. Nekrasov and M. V. Sadovskii, JETP Lett. **96**, 227 (2012).
[13]H. Chen, X.-F. Xu, C. Cao, and J. Dai, Phys. Rev. B **86**, 125116 (2012).
[14]C.-J. Kang, K.-H. Ahn, K.-W. Lee, and B. I. Min, arXiv:1207.6196.
[15]F. Marsiglio and J. P. Carbotte, Phys. Rev. B **33**, 6141 (1986).
[16]S. Baroni, S. de Gironcoli, A. Dal Corso, and P. Giannozzi, Rev. Mod. Phys. **73**, 515 (2001).
[17]P. Giannozzi, S. Baroni, N. Bonini, M. Calandra, R. Car, C. Cavazzoni, D. Ceresoli, G. L. Chiarotti, M. Cococcioni, I. Dabo *et al.*, J. Phys.: Condens. Matter **21**, 395502 (2009).
[18]D. Vanderbilt, Phys. Rev. B **41**, 7892 (1990).
[19]http://www.wien2k.at
[20]O. K. Andersen, Phys. Rev. B **12**, 3060 (1975).
[21]We carefully checked the convergence of our phonon spectra, in particular at the X point, but found no indication of instabilities. The difference most likely stems from the different pseudopotentials employed in their work.
[22]J. P. Carbotte, Rev. Mod. Phys. **62**, 1027 (1990).
[23]O. V. Dolgov, R. K. Kremer, J. Kortus, A. A. Golubov, and S. V. Shulga, Phys. Rev. B **72**, 024504 (2005).